AIAA Propulsion and Energy Forum
10-12 July 2017, Atlanta, GA
53rd AIAA/SAE/ASEE Joint Propulsion Conference

Thrust Assessment for a Laser Tractor Beam Target

John E. Sinko[1]
Department of Physics & Astronomy, St. Cloud State University, St. Cloud, MN 56301
The Institute for Materials, Energetics, and Complexity, St. Cloud, MN 56301

Tyler R. Baxter[2]
Department of Physics & Astronomy, St. Cloud State University, St. Cloud, MN 56301

Mark Gill[3]
Visualization Lab, St. Cloud State University, St. Cloud, MN 56301

and

C. Adam Schlecht[4]
The Institute for Materials, Energetics, and Complexity, St. Louis, MO 63130

This study developed cooperative targets for laser tractor beam retrieval of macroscopic objects in space, for example astronauts and defunct satellites. The present concept is an evolutionary step beyond previous studies on bilayer propellant films, in that the units can be form-fitted around an object, rather than as a separate target extended from the object. A simple analytical model was developed and used to predict chamber pressure and thrust, assuming a gas-producing chemical decomposition reaction. Prototype propellant chambers were developed and 3D-printed for tests in air and under reduced pressure. A carbon-doped sodium bicarbonate-based propellant was tested within one chamber. For continuous tests, the target was irradiated with a 514.5 nm continuous wave argon laser beam. No thrust was observable. For pulsed tests, an Nd:YAG laser beam irradiated the target at 1064 nm and 90 μs pulse length. Thrust, impulse, and mass removal were assessed for the pulsed experiment, and compared with predictions from the analytical model. The experimental results so far reaffirm that scaling to a practical device is achievable.

Nomenclature

Φ	=	Radiant flux (power) of the laser beam just before reaching the target, W
γ	=	Ratio of specific heats
η	=	Dynamic viscosity, Pa
μ	=	Areal mass density, kg m^{-2}
ρ	=	Density, kg m^{-3}
σ	=	Standard deviation
τ	=	Transmittance
τ_L	=	Laser pulse length, s
c_g	=	Specific heat of gaseous propellant, J kg^{-1} K^{-1}
c_s	=	Specific heat of solid propellant, J kg^{-1} K^{-1}
cw	=	Continuous wave

[1] Assistant Professor, Dept. of Physics & Astronomy, 309 Wick Science Building, St. Cloud State University, 720 4th Avenue South, St. Cloud, MN 56301, Member.
[2] Undergraduate student, Dept. of Physics & Astronomy, 324 Wick Science Building, St. Cloud State University, 720 4th Avenue South, St. Cloud, MN 56301, Student Member.
[3] Visualization Engineer, SCSU Visualization Lab, ISELF 101, St. Cloud State University, 720 4th Avenue South, St. Cloud, MN 56301, Nonmember.
[4] Director, Institute of Materials, Energetics and Complexity, St. Louis, MO, 63130, Nonmember.

C_m = Momentum coupling coefficient, N s J^{-1}
E = Laser pulse energy, J
E_a = Activation energy, J mol^{-1}
f_{res} = Resonant frequency, Hz
F = Generic force function, N
g = Gravitational acceleration at the surface of Earth, m s^{-2}
I_{sp} = Specific impulse, s
J = Total impulse, μN s
k_B = Boltzmann constant, J K^{-1}
l = Length of exhaust tube, m
L_d = Heat of decomposition, J kg^{-1}
m = Mass, kg
M = Mach number
M_p = Average particle mass of ablatants, kg
P = Pressure within the tractor beam target chamber, Pa
P_0 = Ambient pressure outside of the tractor beam target, Pa
P_s = Steady state pressure within the tractor beam target, Pa
Q = Laser-induced heat delivered to the propellant mix, J
r = Radius of exhaust tube, m
rms = root mean square
RC = Resistor-capacitor
t = Time, s
T = Temperature within the ablation chamber, K
T_d = Characteristic temperature of decomposition for a propellant, K
v_e = Exhaust velocity, m s^{-1}
V = Volume of the ablation chamber, m^3

I. Introduction

Expanding human presence into the solar system will require innovation in space architecture. One example is development of novel safety infrastructure. NASA Strategic Objective 1.1 seeks to "Expand human presence into the solar system and to the surface of Mars to advance exploration, science, innovation, benefits to humanity, and international collaboration."[1] Besides measures such as tethers and mobile thruster units, a possible addition to safety measures is a laser tractor beam.

A separate problem in modern spaceflight is the so-called 'Kessler Syndrome,' an uncontrolled cascade of space debris which could, for all practical purposes, deny access to space.[2] Laser propulsion has been analyzed as a potential solution to this problem.[3-5] Using a cooperative tractor beam system, a relatively low-power ground-based laser could cooperatively de-orbit satellites at the end of life while minimizing interference with other orbital assets.

Preceding studies on laser tractor beams achieved macroscopic, attractive thrust using similar laser propulsion methods.[6-8] Other efforts used laser thrusters to prevent redeposition on optics.[9] Previous work includes a conceptual proposal on 'laser tractor-beam' methods for the retrieval of astronauts.[10] Successive preliminary experimental studies of bilayer propellants demonstrated functional, switchable thrust for a single target with small numbers of pulses[11]. Primary attempts during these studies were to design further complex propellant configurations; however, a suitable composite target was not achieved, primarily because of catastrophic target damage ensuing from the ablation event, and more generally because no convenient option existed for coupling a bipropellant film 'receiver' to a payload[12]. A further significant challenge in this line of research is developing a reusable propellant concept with acceptable thrust capability at 'safe' laser power levels to avoid collateral damage to assets or injury to astronauts.

II. Analytical Model Development for a Propellant Pack

We assess the viability of cooperative laser propulsion 'tractor beam' based on total thrust for continuous wave (cw) laser propulsion or imparted impulse for pulsed propulsion. Most generally,

$$I = \int_{t_1}^{t_2} F(t)dt \, . \tag{1}$$

F(t) is some function representing force (thrust) as a function of time. We avoid the presupposition that cw laser-generated force is constant. Whether in continuous or pulsed operation, the laser propulsion researcher should diligently measure the time-dependent force. The momentum coupling coefficient is defined as impulse divided by laser pulse energy:

$$C_m = \frac{I}{E}, \tag{2}$$

and the specific impulse is defined as:

$$I_{sp} = \frac{I}{mg}, \tag{3}$$

where m is the mass ablated by a single laser pulse.

A simplified, schematic laser-driven propellant chamber is depicted in Fig. 1. For continuous irradiation, laser power P_L arrives at the target and passes through a front optical surface (and pressure membrane). Propellant material within the chamber is heated and vaporized, following the typical thermodynamics for materials. We focus on a decomposition process with latent heat of decomposition L_d and specific heats c_s and c_g for the solid and gas phases, respectively. Thermal losses to the chamber are ignored and 100% absorption of laser energy reaching the propellant is assumed for removal of propellant mass m. Although such reactions often have an activation energy requirement E_a, this energy is returned to the system, whereas the heat of decomposition is used in the decomposition process. Then the net heat for the decomposition as an ongoing process is:

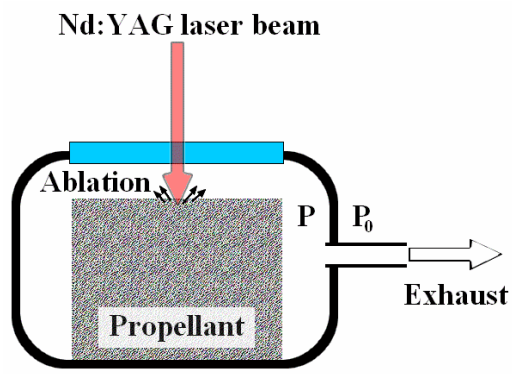

Figure 1. Propellant chamber concept.

$$Q = mc_s\Delta T + mL_d + mc_g\Delta T. \tag{4}$$

Many propellants have been explored in the laser propulsion literature ranging from liquids to polymers, and even powders[13]. Although significant thrust can be realized by including chemical energy in the propellant[14], sometimes propellant design for laser propulsion argues for an efficient direct path from the solid to the gaseous state. Propellants which undergo chemical decomposition to generate gas at low temperature are of special interest. Ammonium carbonate ($(NH_4)_2CO_3$) is one such substance that decomposes to ammonia, carbon dioxide, and water when heated. Sodium bicarbonate ($NaHCO_3$) is another example and evolves carbon dioxide when heated. Table 1 assembles thermodynamic properties of the two mentioned propellant candidates.

We note that $L_d \gg c_s\Delta T + c_g\Delta T$ as long as $\Delta T \ll 1000$ K. Based on the T_d data in Table 1, we may reasonably assume this condition will be met. The rate of change of propellant mass can then be approximated as:

Table 1. Characteristic values for representative propellant materials[15-18].

Substance	M_p [g/mol]	L_d [kJ mol^{-1}]	L_d [J g^{-1}]	E_a [kJ mol^{-1}]	T_d [K]
Ammonium carbonate	96.1	189.8±4.1 191.7±4.5 181.4±12.2 205±19	1975±43* 1995±47* 1888±127* 2133±198*	85.73±6.02	353-393 333-393
Sodium bicarbonate	84.0	135.2	1203 ± 5 1610.*	101.1±0.5	365-405

*calculated from the first two columns

$$\frac{dm}{dt} \approx \frac{1}{L_d}\frac{dQ}{dt} = \frac{\Phi}{L_d}. \tag{5}$$

Throughout this work we assume this term is a constant source term driving up pressure in the chamber in cw mode, and we assume exhaust is ideal gas at steady-state temperature T_g. The ideal gas law relates m and P as:

$$P = \frac{m}{M_p V} k_B T = n k_B T \,. \tag{6}$$

If molecular effusion is the predominant mechanism of exhaust, then mass flow loss rate is:

$$\frac{dm}{dt} = \frac{M_p V}{k_B T}\frac{dP}{dt} = -\frac{\pi r^2 M_p P}{\sqrt{2\pi M_p k_B T}} = -\frac{r^2 P\sqrt{\pi M_p}}{\sqrt{2k_B T}} \tag{7}$$

so that:

$$\frac{dP}{dt} = \frac{k_B T}{M_p V}\frac{\Phi}{L_d} - \frac{r^2\sqrt{\pi k_B T}}{V\sqrt{2M_p}} P \tag{8}$$

As a first order loss term, this suggests pressure rise within the chamber is exponentially governed:

$$P(t) = \frac{\Phi\sqrt{2k_B T}}{L_d r^2\sqrt{\pi M_p}}\left(1 - e^{-\frac{r^2\sqrt{\pi k_B T}}{V\sqrt{2M_p}}t}\right) \tag{9}$$

suggesting a steady-state pressure of:

$$P_s = \frac{\Phi\sqrt{2k_B T}}{L_d r^2\sqrt{\pi M_p}} \tag{10}$$

Ignoring redeposition, conservation of mass restricts propellant exhaust to a mass flow rate of:

$$\frac{dm}{dt} \approx \rho A v_e \approx n M_p A v_e = \frac{\pi r^2 P M_p}{k_B T} v_e \tag{11}$$

where $P = P_s$ corresponds to the peak mass flow rate. Therefore the exhaust speed is limited to:

$$v_e = \frac{\Phi k_B T}{\pi r^2 P_s M_p L_d} = \sqrt{\frac{k_B T}{2\pi M_p}} \tag{12}$$

The exhaust gases include components of ammonia, carbon dioxide, and water vapor, providing favorable entropy for the reaction and a large volume expansion due to the number of moles of gas produced:
$(NH_4)_2CO_3 \rightarrow 2NH_3(g) + CO_2(g) + H_2O(g)$

The sound speed for an ideal gas is:[19]

$$c_s = \sqrt{\frac{\gamma P}{\rho}} = \sqrt{\frac{\gamma k_B T}{M_p}} \tag{13}$$

To characterize the exhaust flow of such gases, the values for the heat of decomposition, specific heat, and dynamic viscosity are of interest, and are assembled in Table 2.

Table 2. Characteristic values for representative exhaust gases around 400 K.[20-23]

Gas	C_p [J kg^{-1} K^{-1}]	C_v [J kg^{-1} K^{-1}]	γ [-]	M_p [kg]	c_s [m s^{-1}]	v_e (Eq. 12) [m s^{-1}]	η [Pa s]
CO_2	844	655	1.29	7.308×10^{-26}	312	110.	1.5×10^{-5}
H_2O	2190	1660	1.32	2.992×10^{-26}	494	171	9.7×10^{-6}
NH_3	1930	1460	1.32	2.828×10^{-26}	508	176	9.8×10^{-6}

One objective of our work is the prediction of thrust from a laser tractor beam target chamber, in the context that our concept is to use hundreds to thousands of chambers to multiply the thrust from a single unit. We may invoke Newton's laws:

$$F = \left|\frac{dm}{dt}v_e\right| = \frac{r^2 P\sqrt{\pi M_p}}{\sqrt{2k_B T}}\sqrt{\frac{k_B T}{2\pi M_p}} = \frac{r^2 P_s}{2} = \frac{\Phi\sqrt{k_B T}}{L_d\sqrt{2\pi M_p}}. \quad (14)$$

This result implies that thrust from the target chamber will increase directly with delivered laser power, or for a laser source with constant irradiance, will increase directly with the total area of the receiver units.

III. Experiment and Methods

A. Experiment Setup for Laser Ablation and Force Measurement

The focus of this study is an experimental investigation into test chamber designs consistent with cooperative 'tractor beam' propulsion. We intended to test and refine an initial prototype tractor beam target. The imagined application is space asset retrieval; thus, we focused on testing our target chambers under vacuum. A multi-format ISO80/CF4.5"/CF2.75" 6-way cross formed the core of a small vacuum chamber that served as our main test area for laser irradiation of the prototype chambers. For these experiments, rough vacuum conditions ranging from 0.3 Pa to 101,325 Pa were produced with a rotary vane pump (Ulvac Kiko, GLD-136C) and the pressure was monitored via a Pirani gauge (Kurt J. Lesker, 275i). The system had a turbo-drag pump that can reach much lower pressures; we hope to explore ambient pressure effects in future work.

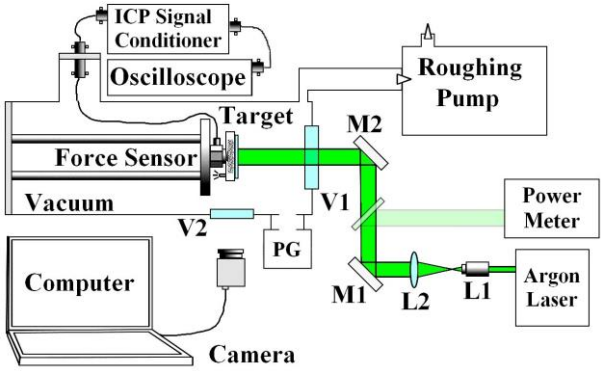

Figure 2. Experimental setup diagram for cw tests with argon laser.

The experiment setup for cw mode is shown in Fig. 2. An argon ion laser (SpectraPhysics Stabilite 2017) produced a 514.5 nm beam with adjustable power up to approximately 2 W, nominal beam divergence 0.5 mrad, and nominal beam diameter 1.4 mm. The beam was passed through a collimating telescope (L1 and L2), reflected off of mirror group M1, and was split at the beamsplitter between M1 and M2 for power detection, then reflected off of mirror group M2 before passing into the chamber at viewport V1. Beam power was measured internally and with a thermal detector (Thorlabs S401C with PM200) placed to intercept the low power beam split off by the beamsplitter. Power calibration measurements are shown in Fig. 3. The middle line in the figure is the expected 1:1 calibration; the actual laser output at the aperture was higher by about 23%, but by the time the beam reached the target, only 54% of the internally measured power was present. The beam entered the vacuum chamber through a Kodial™ glass viewport V1 at normal incidence before arriving at the target. Eight percent total beam reflection losses through this window were assumed, based on normal incidence Fresnel reflectivity with an index of refraction of 1.5 for the glass

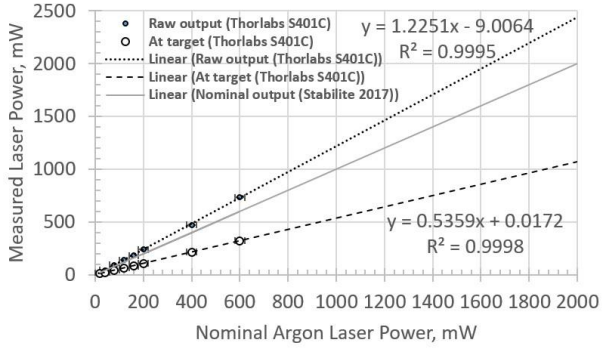

Figure 3. Nominal vs. measured cw power output for the argon ion laser.

and 1 for air. The instrument marked 'PG' is the Pirani gauge.

For the pulsed experiments, an Nd:YAG laser (Continuum YG660) was operated at 1.064 μm wavelength and pulse energies up to 101 ± 2 mJ (rms, 100 pulses). The overall pulsed setup is shown in Fig. 4. The laser can be operated in single pulse mode or in repetitively pulsed mode at 20 Hz. As in the cw tests, a beamsplitter was used to monitor the energy for each shot by splitting off 18.2% ± 0.6% of the beam power into a laser energy detector (Gentec-EO QE25LP-H-MB-D0 with Maestro™ meter). A Thorlabs DET10A silicon photodiode detector (PD) with 200-1100nm spectral response and 1 ns rise time caught reflections from the power meter to optically trigger recording of the signal from the force sensor.

For a visual record, a machine vision camera (FLIR/Point Grey Flea3) attached to a laptop visually monitored the ablation process through viewport V2.

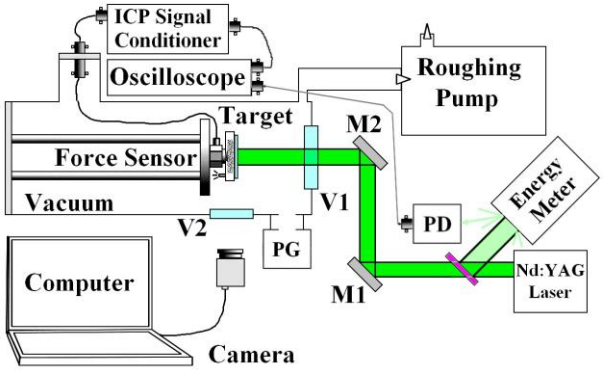

Figure 4. Experimental setup diagram for pulsed tests with Nd:YAG laser.

A technical problem prevented the use of the Q-switch for this experiment; a pulse length of 90 ± 10 μs FWHM was measured using the photodiode. The beam entered the vacuum chamber through a glass viewport. Beam energy was measured after passing through the viewport at 85.0 ± 0.6 mJ (rms, 30 pulses).

For measurement of force and impulse, targets were attached to an integrated circuit piezoelectric (ICP) force sensor (PCB Piezotronics, 208C01, 0.112410 N/V) with a BeCu stud (PCB Piezotronics, 081B05). The aluminum mount surface beneath the sensor was prepared by manual polishing to flat 1500 grit. The electronic signal couples out by way of a BNC flange to a 12-bit, variable current, unity gain, 16-channel ICP signal conditioner (PCB Piezotronics, 481A01-080) and then to a 4-channel digital storage oscilloscope (Tektronix 2024B, 200MHz, 2GS/s, 2500 samples). Our resolution step is around 5 mV for this system, corresponding to a force detection threshold of about 44 mN. However, using triggered sample averaging of up to 128 samples in pulsed mode, the noise floor can be reduced to roughly 3.9 mN. In both cw and pulsed testing, besides approaching the root mean square (rms) noise floor, we encountered several undesirable experimental artifacts which had the potential to mask or distort our experimental signals. Figure 5 illustrates two of these undesirable artifacts.

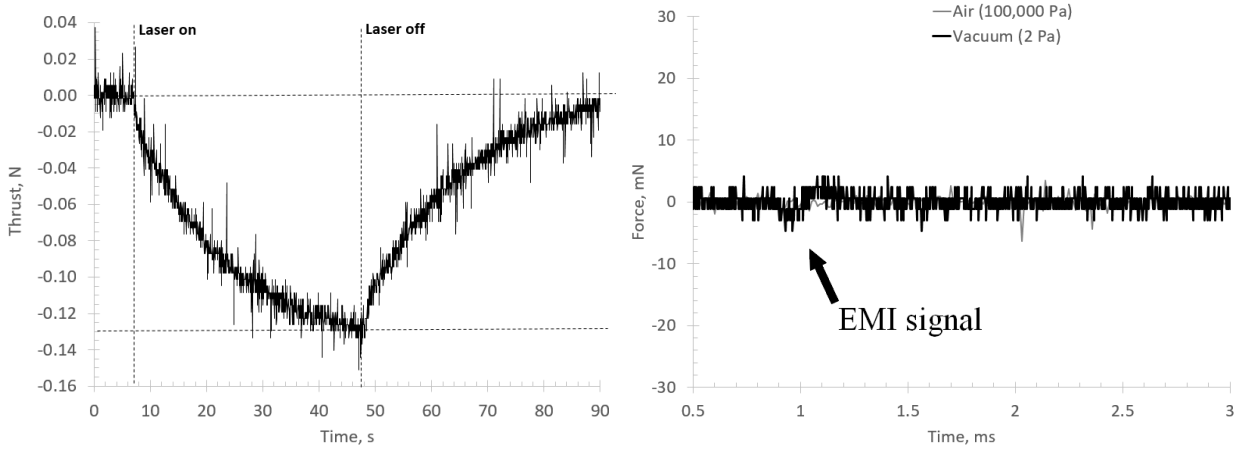

(a) **(b)**

Figure 5. False thrust signals (a) due to secondary pyroelectric effect under cw irradiation; (b) due to electromagnetic interference from the Nd:YAG laser during pulsed tests.

The signal in Fig. 5(a) is generated by the force sensor, but is an indirect measurement of temperature, not force. The temperature increase gives rise to the secondary pyroelectric effect or "pyroelectric effect at constant strain," i.e. thermal expansion of the quartz crystal produces a signal consistent with a negative (tensile) force measurement.[24,25] For these cw tests, a polyamide post was machined and inserted between the force sensor and the target to thermally isolate the force sensor from the target and minimize false signals. In Fig. 5(b), a different sort of false signal is present. During pulsed tests with the YAG laser, the 1064 nm laser beam was intentionally blocked by an opaque steel screen

placed in front of the vacuum chamber. The flashlamp energy discharge generates enough radio frequency emissions to cause a spurious peak on the signal from the force sensor.

B. Cooperative Target

The tractor beam target chamber used in this experiment was designed in Solidworks™ and constructed in white acrylonitrile butadiene styrene (ABS) plastic on a 3D printer (Lulzbot® Taz 6). The rear surface was tapped for UNC 10-32 to facilitate mounting and installation with the force sensor on a BeCu stud. Four roughly circular exhaust holes of ≈0.8 mm radius were drilled with a Dremel® tool using a 1/16" bit. Propellant material was produced as a mixture of 80% sodium bicarbonate powder with 20% carbon powder by mass. This mixture was combined with Loctite® Go2® Gel, an organosilane-based resin, applied inside the chamber, and allowed to cure for 24 hours. The chamber was then sealed with a 22 mm × 22 mm × 0.15 mm glass plate, attached to the top of the chamber by unmodified resin.

Mass measurements were conducted before and after laser irradiation using a Mettler AE163 scientific balance with 10 μg resolution and approximately ±30 μg measurement repeatability. For measurements of target mass before laser irradiation, the samples sat overnight under vacuum conditions at ≈10 Pa to eliminate systematic mass measurement errors from offgassing.

C. Pressure, Mass Flow, Exhaust Speed, and Thrust Simulations

To test the theoretical developed in the Introduction, experimental parameters were inserted into the equations to forecast chamber pressure, mass flow rate, exhaust speed, and thrust. Experimental parameters are presented in Table 3. These parameters were inserted into the model with the gas data in Table 1 to predict pressure in the target chamber and force generated during irradiation.

Table 3. Experimental Parameter Values.

Parameter	Value	Uncertainty (1 σ)
A	1.00×10^{-4}	0.01×10^{-4}
l	0.100	0.001
P_0	1.0	0.1
r	4.0×10^{-4}	5×10^{-5}
τ	0.92	0.01
T_0	295	1
V	2.288×10^{-6}	9×10^{-9}

To predict chamber propulsive behavior, we focused on a few key parameters, illustrated in Fig. 6(a) and 6(b). The 10-90% rise time of the predicted pressure and force is approximately 1.2 ms. The pressure rise is predicted to be around a few hundred Pascal at 2 W laser power for an exhaust tube of around 1 mm radius. As shown in Fig. 6(a), decreasing the radius of the exhaust tube results in higher chamber pressure

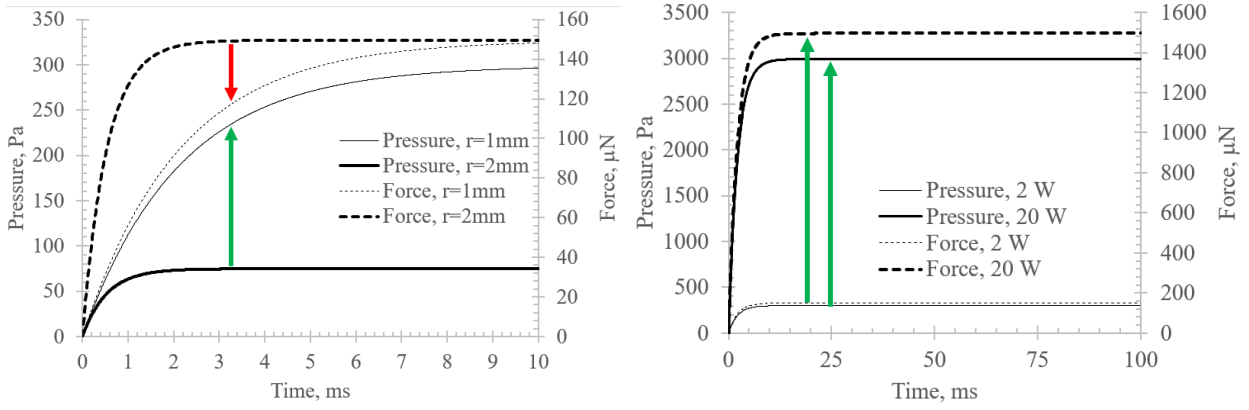

(a) **(b)**

Figure 6. Pressure and force for (a) two exhaust tube radii, both under 2 W laser irradiation, and (b) two laser power conditions, both for a 1 mm radius exhaust tube.

but lower peak force. It may be beneficial to design the chamber with a larger exhaust tube radius. This prediction is counter to our initial expectations. Fig. 6(b) illustrates that pressure and force scale directly with applied laser power. Unfortunately, the thrust scenarios predicted under continuous irradiation conditions remain roughly a factor of 50 below the detection threshold of the force sensor (i.e., at most, around 0.1 mN). Importantly, this limitation represents no dead end in terms of the development of tractor beam target units, since the final version would be scaled up to a 100 × 100 grid of around 10^4 total units, i.e. on the order of 1 N under a kW-class laser beam.

What about the pulsed case? If the same processes are generating thrust, which may not actually be the case, the primary differences are the shorter laser pulse length (90 μs) and increased peak power (≈1 kW). If we enter these laser pulse parameters into the model as a constant 1 kW for 90 μs (i.e., a 90 mJ pulse), we observe the behavior illustrated in Fig. 7. The model predicts generation of a signal that may be experimentally observable if averaging is used. Increasing the exhaust tube radius significantly might allow detection of the thrust signal without averaging; however, the threshold for detection is predicted at an exhaust tube radius around 8 mm. A hole of this radius would a significant fraction of the rear area of the target.

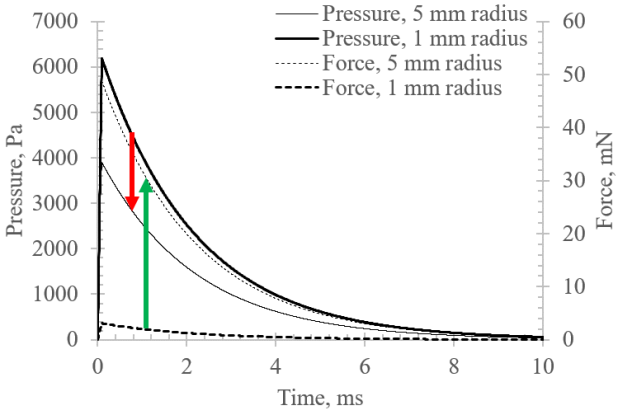

Figure 7. Pressure and force for two laser power conditions, both for a 1 mm radius exhaust tube.

By integrating to find the area under the curve for the pulsed case, the impulse per shot can be estimated. For the 1 mm radius case (≈3 mm^2), the model predicts only about 7 μNs, which corresponds to ≈80 μNs/J; however, when the radius is increased to 5 mm (≈79 mm^2), the imparted impulse prediction rises to around 110 μNs. The momentum coupling coefficient is then predicted at ≈1300 μNs/J. The mass removal may be anticipated based on the 90 mJ laser pulse and the data in Table 1 as approximately 60-70 μg per shot, considering only the heat of decomposition. The predicted I_{sp} is then approximately 10-13 s for the 1 mm radius case, or 150-200 s for the 5 mm radius case. While these values do not push the known bounds of laser propulsion performance, they are likely adequate for our application.

Some discussion of the limitations of the model is appropriate. The effects of target heating are likely to become important for the pulsed laser irradiation case, although the model so far neglects those effects. In addition, nonequilibrium effects such as shock waves and generation of debris particles are likely in the pulsed experiment, and such effects are neglected by our model. Further development of cooperative tractor beam target models must likely proceed without the confines of a purely analytical approach. Numerical model development seems promising.

IV. Experimental Results and Discussion

Results are presented below for both continuous and pulsed operation.

A. Continuous Tests

As discussed in the previous section, simulations of the force and pressure generated in the test environment assuming continuous irradiation implied that the level of thrust would be below the detection threshold of the force sensor. Our initial investigation initially seemed to surpass this expectation, as the result illustrated in Fig. 5(a) would have indicated ≈1600% ablation efficiency. The responsible mechanism is the secondary pyroelectric effect; i.e., thermal expansion results in a tensile piezoelectric signal detection. This is an uncalibrated temperature measurement of the sensor rather than a calibrated force measurement of the target. For the pulsed tests, this effect is easily distinguished from the force signal, since the time scale is roughly 10^5–10^6× longer than the laser irradiation. For the continuous tests, it is less clear whether such thermal effects can be successfully separated from the force measurements since the two phenomena exist over similar time scales. The analytical model predicted a rise time of approximately 1 ms under constant irradiation, so it may still be possible to observe the onset of the force signal, given sufficiently sensitive equipment. With our current laboratory setup, we could not detect any definite force signal under continuous laser irradiation at the maximum laser beam power of 2 W.

B. Pulsed Tests

Our second set of tests involved pulsed Nd:YAG laser ablation at 1.064 μm. Based on the model in part II, pulsed tests could generate detectable peak force and imparted impulse. Dividing the laser energy of about 100 mJ into its roughly 100 μs pulse length yields approximately 1 kW average power, about 10^3× more than the cw laser power. However, when the experiment began, it remained unclear whether a signal would be observed from the force sensor.

In Fig. 8, we present results for irradiation of the target discussed in the introduction at atmospheric pressure and at a reduced pressure of 2.0 Pa. A signal was detected in the experiment, as compared with the beam-blocked case

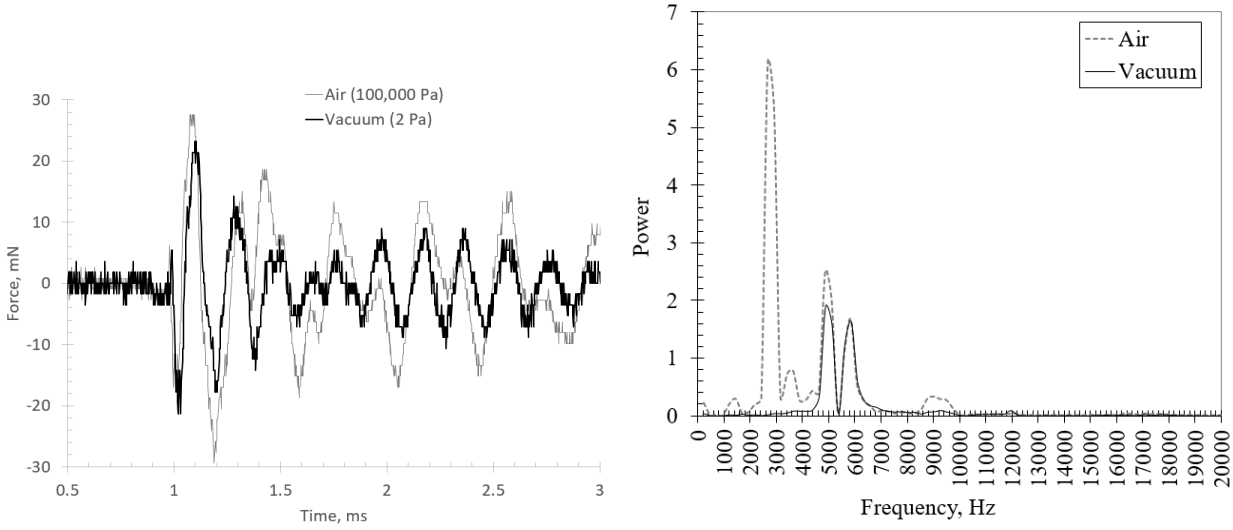

(a) **(b)**

Figure 8. Experimental results: (a) force signal in air and under vacuum; (b) corresponding power spectra.

illustrated earlier in Fig. 5(b). At face value, the signal in Fig. 8(a) appears to be a 20-30 mN amplitude, damped oscillation with primary period near 200 μs. Fast Fourier transform power-frequency spectra are presented in Fig. 8(b), and reveal oscillation frequencies around 2.7, 4.9, and 5.9 kHz for air, and 4.9 and 5.9 kHz for the reduced pressure case. The largest oscillation present in the air case is absent under vacuum and therefore is likely to arise from acoustic resonance of the air inside the chamber. The origin of the other two peaks is likely to be oscillations within the solid structure of the target. The strength of these three oscillations dwarfs that of the signal, and therefore the data in Fig. 8 must be approached with some caution. In principle, the bandwidth of both the force sensor and the electronic measurement system can also contribute to limiting detection and linearity of the sensor. Therefore, it is not clear whether the response of the sensor can be validly interpreted as a quantitative (but rough) measurement of impulse, or if the detection is distorted due to nonlinear response. The observed frequencies are well above the minimum usable frequency, which based on the RC time constant of the sensor is around 10 mHz. The resonant frequency of the force sensor given by the manufacturer is 36 kHz. The coupling of the target to the sensor leads to a new resonant frequency of the sensor-target system. This resonance was separately interrogated by manually striking the sensor-target system with several small rods of different materials, which indicates a modified resonant frequency around 3.6 kHz. A common rule of practice is to use one third or one fifth the resonant frequency as a frequency limit, which holds errors in spectral content to around 10-20%.[26,27] In our experiment, the upper frequency limit is therefore restricted to around 0.7-1.2 kHz. Little signal remains after this cutoff is applied to the data, but integration of the filtered data can roughly estimate impulse. For both air and vacuum cases, the amplitude of this estimated impulse is on the order of 1-2 μNs. Given the 85 mJ pulse energy, and assuming 4% losses for each surface of the glass seal plate, the momentum coupling coefficient in this process would be inferred as approximately 10-30 μNs/J, which is significantly lower than the predictions of the analytical model. This discrepancy might arise from several sources; for example, propellant heating, thermal diffusion, the influence of the resin, or the reduction of ablatable material brought about by including carbon in the propellant mixture.

The mass of the target was measured before and after the test, resulting in a decrease from 5.75804 ± 0.00015 g before the experiment to 5.75589 ± 0.00009 g after the experiment. A total of 266 total laser shots were conducted, so the difference between these values can be calculated as 8.1 ± 0.7 μg/shot, with an assumption that the rate of mass removal does not greatly vary from shot to shot. This value is only a fraction of the 60-70 μg predicted using the heat of decomposition alone, and the same sources as mentioned above in the previous paragraph may be responsible for the difference. The calculated specific impulse is approximately 13 s. This result is consistent with the value calculated from the v_e/g form of specific impulse using the thermal gas speed of carbon dioxide in Table 2. The speed is also of the same order of magnitude as predicted by the analytical model.

For future tests, we observe several pathways for improvement. First, we intend to acquire a force sensor with a higher resonant frequency and greater sensitivity. Second, we plan to conduct tests of new targets with size and mass

chosen to avoid this resonant condition. Third, we intend to increase our laser capabilities to deliver more energy to the targets for testing. Fourth, we are interested in exploring chemically energetic propellants. Finally, we are developing torsion and hanging impulse pendula in our laboratory and intend to conduct independent measurements in air and under vacuum.

V. Conclusions

The goal of this study was to further develop cooperative laser tractor beam prototype targets in service of achieving a practical system to remotely retrieve space assets, such as astronauts and satellites. A simple model was developed for chamber pressure, exhaust velocity, thrust, and impulse from cooperative tractor beam targets. Predictions for propulsion performance were made based on the model. A prototype tractor beam target chamber was designed and 3D-printed. A sodium bicarbonate-based propellant was incorporated into a tractor beam target chamber and irradiated by an argon laser in continuous mode, and separately by an Nd:YAG laser in pulsed mode. Thrust, impulse, and ablated mass were analyzed to assess propulsion performance in both air and under vacuum. No thrust was detected in the continuous experiments, but an impulse was estimated based on the results of the pulsed experiments which is in rough agreement with the predictions of the analytical model. The momentum coupling coefficient and specific impulse were also calculated. The experiment generally supports the idea that scaling up is feasible. Additional testing is necessary to confirm the experimental results, and to extend the laboratory testing to higher laser pulse energies.

Acknowledgments

This work is supported by a 2015 SCSU University Researcher Award, a 2016 SCSU New Researcher Award, and a 2016 SCSU Student Researcher Award. Support was also provided by the SCSU Dept. of Physics & Astronomy and the SCSU Dept. of Chemistry & Biochemistry, the SCSU Visualization Laboratory, and by the Institute for Materials, Energetics, and Complexity (IMEC). Heartfelt appreciation is extended for contributions to the research from students including Eu Sheng Chung, Alexis Corbett, Chris Crawford, David Corgard, Eliakim Balle, Sam Hartman, and James Sweeney.

References

[1]National Aeronautics and Space Administration, "NASA Strategic Plan 2014", pp. 3 and 11, 2014.

[2]Kessler, D. J. and Cour-Palais, B. G., "Collision Frequency of Artificial Satellites: The Creation of a Debris Belt," *Journal of Geophysical Research*, Vol. 83, No. A6, 1978, 2637-2646.

[3]Phipps, C., "LISK-BROOM: A laser concept for clearing space debris," *Laser and Particle Beams*, Vol. 13, No. 1, 1995, pp. 33-41.

[4]Phipps, C. R., Albrecht, G., Friedman, H., Gavel, D., George, E. V., Murray, J., Ho, C., Priedhorsky, W., Michaelis, M. M., and Reilly, J. P., "ORION: Clearing near-Earth space debris using a 20-kW, 530-nm, Earth-based, repetitively pulsed laser," *Laser and Particle Beams*, Vol. 14, No. 1, 1996, pp. 1-44.

[5]Beiting, E. J., "Orbital Debris Removal by Ground-based Laser Ablation: An Overview," Aerospace Report No. TOR-2010(1189)-1, 2010.

[6]Yokoyama, S., Horisawa, H., Funaki, I., and Kuninaka, H., "Fundamental Study of Laser Micro Propulsion Using Powdered-Propellant," *International Electric Propulsion Conference* [online proceedings], ERPS, Fairview Park, OH, 2007, pp. 1-7, URL: http://erps.spacegrant.org/uploads/images/images/iepc_articledownload_1988-2007/2007index/IEPC-2007-230.pdf [cited 14 June 2017].

[7]Ohkubo, T., Yabe, T., Baasandash, C., Taniguchi, K., Miyazaki, S., and Ogata, Y., "Near Term Application of Water-Powered Laser-Propulsion," *35th AIAA Plasmadynamics and Lasers Conference*, AIAA, Washington, DC, 2004, pp. 1-8.

[8]Egorov, M. S., Rezunkov, Yu. A., Repina, E. V., and Safronov, A. L., "Laser corrective propulsion plant for spacecraft," *Journal of Optical Technology*, Vol. 77, No. 3, March 2010, pp. 159-164.

[9]Phipps, C. R., Luke, J. R., McDuff, G. G., and Lippert, T., "Laser-driven micro-rocket," *Applied Physics A*, Vol. 77, No. 2, 2003, pp. 193-201.

[10]Sinko, J. E., "Laser Ablation Propulsion Tractor Beam System," *Journal of Propulsion and Power*, Vol. 26, No. 1, Jan.-Feb. 2010, pp. 189-191.

[11]Sinko, J. E. and Schlecht, C. A., "CO_2 Laser Ablation Propulsion Tractor Beams," *Proceedings of the 6th International Symposium on Beamed Energy Propulsion*, ed. C. Phipps, K. Komurasaki, and J. Sinko, AIP Conference Proceedings, Melville, NY, Vol. 1230, No. 1, 2009, pp. 282-294.

[12]Sinko, J., Schlecht, C., Lis, T., Davidson, R., Gregory, D., Yokota, S., Harada, S., Sasoh, A., Oh, B., and Larus, M., "Laser Ablation Tractor Beaming with Bilayer Targets," *50th AIAA Aerospace Sciences Meeting*, AIAA, Washington, DC, 2012.

[13]Phipps, C., Birkan, M., Bohn, W., Eckel, H.-A., Horisawa, H., Lippert, T., Michaelis, M., Rezunkov, Y., Sasoh, A., Schall, W., Scharring, S., and Sinko, J., "Review: Laser-Ablation Propulsion," *Journal of Propulsion and Power*, Vol. 26, No. 4, 2010, pp. 609-637.

[14]Phipps, C., Luke, J., Funk, D., Moore, D., Glownia, J., and Lippert, T., "Laser impulse coupling at 130 fs," *Applied Surface Science*, Vol. 252, No. 13, 2006, pp. 4838-4844.

[15]Muehling, J. K., Arnold, H. R., and House, J. E. Jr., "Effects of particle size on the decomposition of ammonium carbonate," *Thermochimica Acta*, Vol. 255, 1995, pp. 347-353.

[16]House, J. E. Jr., "Decomposition of ammonium carbonate and ammonium bicarbonate and proton affinities of the anions," *Inorganic and Nuclear Chemistry Letters*, Vol. 16, No. 4, 1980, pp. 185-187.

[17]House, J. E. Jr., "A TG Study of the Kinetics of Decomposition of Ammonium Carbonate and Ammonium Bicarbonate," *Thermochimica Acta*, Vol. 40, No. 2, 1980, pp. 225-233.

[18]Hartman, M., Svoboda, K., Pohořelý, M., and Šyc, M., "Thermal Decomposition of Sodium Hydroxide and Textural Features of Its Calcines," *Industrial and Engineering Chemistry Research*, Vol. 52, No. 31., 2013, pp. 10619-10626.

[19]Vincenti, W. G. and Kruger, C. H. Jr., *Introduction to Physical Gas Dynamics*, Krieger Publishing Company, Malabar, FL, 2002, Chap. XII, Sec. 5, 488.

[20]F. L. Smidth, Inc., "Gases - Specific Heat Capacities and Individual Gas Constants," [catalog data], 2017, URL: http://catalog.conveyorspneumatic.com/Asset/FLS%20Specific%20Heat%20Capacities%20of%20Gases.pdf. [cited 13 June 2017].

[21]Fenghour, A., Wakeham, W. A., and Vesovic, V., "The Viscosity of Carbon Dioxide," *Journal of Physical and Chemical Reference Data*, Vol. 27, No. 1, 1998, pp. 31-44.

[22]Teske, V., Vogel, E., and Bich, E., "Viscosity Measurements on Water Vapor and Their Evaluation," *Journal of Chemical & Engineering Data*, Vol. 50, No. 6, 2005, pp. 2082-2087.

[23]Brokaw, R. S., "Viscosity of Gas Mixtures," NASA Technical Note TN D-4496, Apr. 1968.

[24]Cusack, N., *The Electrical and Magnetic Properties of Solids*, Longmans, Green and Co., New York, 1958, Chap. 18.4, pp. 403-404.

[25]Mason, W. P., *Piezoelectric Crystals and Their Application to Ultrasonics*, D. Van Nostrand Company, Inc., New York, Chap. 3, pp. 38-39.

[26]Broch, J. T., *Mechanical Vibration and Shock Measurements*, 2nd ed., Brüel & Kjær, Denmark, 1980, Chap. 6.2, 102.

[27]Walter, P. L., "Selecting Accelerometers for and Assessing Data from Mechanical Shock Measurements," TN-24, PCB Piezotronics, Inc., Buffalo, NY, 2017.